molecules

MDPI

Article

Study on Paramagnetic Interactions of $(CH_3NH_3)_2CoBr_4$ Hybrid Perovskites Based on Nuclear Magnetic Resonance (NMR) Relaxation Time

Ae Ran Lim [1,2,*] and Sun Ha Kim [3,4]

1 Analytical Laboratory of Advanced Ferroelectric Crystals, Jeonju University, Jeonju 55069, Korea
2 Department of Science Education, Jeonju University, Jeonju 55069, Korea
3 Korea Basic Science Institute, Seoul Western Center, Seoul 120-140, Korea
4 Department of Chemistry, Kyungpook National University, Daegu 41566, Korea
* Correspondence: aeranlim@hanmail.net; Tel./Fax: +82-(0)63-220-2514/+82-(0)63-220-2053

Received: 17 July 2019; Accepted: 2 August 2019; Published: 9 August 2019

Abstract: The thermal properties of organic–inorganic $(CH_3NH_3)_2CoBr_4$ crystals were investigated using differential scanning calorimetry and thermogravimetric analysis. The phase transition and partial decomposition temperatures were observed at 460 K and 572 K. Nuclear magnetic resonance (NMR) chemical shifts depend on the local field at the site of the resonating nucleus. In addition, temperature-dependent spin–lattice relaxation times ($T_{1\rho}$) were measured using ^1H and ^{13}C magic angle spinning NMR to elucidate the paramagnetic interactions of the $(CH_3NH_3)^+$ cations. The shortening of ^1H and ^{13}C $T_{1\rho}$ of the $(CH_3NH_3)_2CoBr_4$ crystals are due to the paramagnetic Co^{2+} effect. Moreover, the physical properties of $(CH_3NH_3)_2CoBr_4$ with paramagnetic ions and those of $(CH_3NH_3)_2CdBr_4$ without paramagnetic ions are reported and compared.

Keywords: organic/inorganic hybrid materials; structure; dynamics; $(CH_3NH_3)_2CoBr_4$; MAS/NMR

1. Introduction

Hybrid organic–inorganic compounds based on perovskite structures are currently attracting an increased amount of interest owing to their potential as substitutes for perovskite solar cells [1–10]. However, the toxicity and chemical instability of perovskites continue to be the major problems associated with their use in solar cells. Compounds in the $(CH_3NH_3)_2MX_4$ family (where M is the transition metal and X is halide) exhibit a variety of physical properties [1,11]. Ions of the transition metal M are located in the tetrahedral structure formed by the halogen ions X, and lie in the planes bridged by the $(CH_3NH_3)^+$ cations [12]. These crystals have a layered structure and exhibit quasi-, two-dimensional magnetic properties. Most recently, electrochemical oxygen evolution of $(CH_3NH_3)_2CoBr_4$, a lead-free cobalt-based perovskite, has been reported by Babu et al. [13]. The $(CH_3NH_3)_2CoBr_4$ crystal belongs to the $(CH_3NH_3)_2MX_4$ series and the family of hybrid organic–inorganic compounds in which $(CH_3NH_3)^+$ cations are connected via a bridge structure between the planes that contain the Co^{2+} ions. At room temperature, the $(CH_3NH_3)_2CoBr_4$ crystal structure has monoclinic symmetry and belongs to the space group $P2_1/c$, with lattice constants a = 7.9782 Å, b = 13.1673 Å, c = 11.2602 Å, and ß = 96.3260° [14]. The unit cell contains four formula units and four magnetic Co^{2+} ions. The $(CoBr_4)^{2-}$ units are surrounded by seven $(CH_3NH_3)^+$ cations, and two different crystallographic $(CH_3NH_3)^+$ cations exist. Although the tetrahedral anion exhibits only C_1 symmetry, the deviation from an idealized tetrahedral symmetry is small. The NH_3^+ polar heads of the chains connect the isolated $(CoBr_4)^{2-}$ tetrahedral structure with weak N-H···Br hydrogen bonds. On the other hand, $(CH_3NH_3)_2CdBr_4$ crystals at room temperature have a monoclinic structure and belong to the space group $P2_1/c$ with lattice constants a = 8.1257 Å, b = 13.4317 Å, c = 11.4182 Å, ß = 96.1840°, and Z = 4 [15,16]. The structure of this crystal is very similar

to that of the $(CH_3NH_3)_2CoBr_4$. Until now, the phase transition temperature, thermal property, and paramagnetic interactions of $(CH_3NH_3)_2CoBr_4$ have not been studied in full. The paramagnetic ions of the lead-free perovskite are eco-friendly, which is important for application to solar cells.

The present study was conducted to investigate the thermodynamic properties of the $(CH_3NH_3)_2CoBr_4$ crystal using differential scanning calorimetry (DSC), thermogravimetric analysis (TGA), and optical polarizing microscopy. Additionally, the nuclear magnetic resonance (NMR) chemical shifts and spin–lattice relaxation times $T_{1\rho}$ in the rotating frame of $(CH_3NH_3)_2CoBr_4$ were obtained using ^1H magic angle spinning (MAS) NMR and ^{13}C cross-polarization (CP)/MAS NMR methods at several temperatures to probe the local environments and study the roles of the $(CH_3NH_3)^+$ cations. Moreover, the physical properties of $(CH_3NH_3)_2CoBr_4$ including paramagnetic ions and $(CH_3NH_3)_2CdBr_4$ excluding paramagnetic ions were obtained from previous reports [17], and used as a comparison to understand the effects of Co^{2+} and Cd^{2+} ions.

2. Results and Discussion

TGA and DSC measurements were obtained to understand the thermal stability, structural phase transitions, and melting temperatures. The TGA and DSC curves of $(CH_3NH_3)_2CoBr_4$ are plotted within the temperature range of 300–770 K, as shown in Figures 1 and 2. The transformation anomaly at 460 K (=T_C) in the DSC curve is related to the phase transition. The mass loss of 3.89% occurs at approximately 572 K (=T_d), and is ascribed to the onset of partial thermal decomposition. The compound $(CH_3NH_3)_2CoBr_4$ loses its crystallization at increased temperatures. When comparing the experimental TGA results and possible chemical reactions, the solid residue is calculated on the basis of Equations (1) and (2):

$$(CH_3NH_3)_2CoBr_4 \rightarrow (CH_3NH_2{\cdot}HBr)_2CoBr_2 \rightarrow (CH_3NH_2)_2CoBr_2\ (s) + 2HBr\ (g) \quad (1)$$

Residue: $[(CH_3NH_2)_2CoBr_2$ (M = 280.857 g)]/$[(CH_3NH_3)_2CoBr_4$ (M = 442.681 g)] = 63.4%

$$(CH_3NH_3)_2CoBr_4 \rightarrow (CH_3NH_2{\cdot}HBr)_2CoBr_2 \rightarrow CoBr_2\ (s) + 2(CH_3NH_2{\cdot}HBr)\ (g) \quad (2)$$

Residue: $[CoBr_2$ (M = 218.741 g)]/$[(CH_3NH_3)_2CoBr_4$ (M = 442.681 g)] = 49.4 %

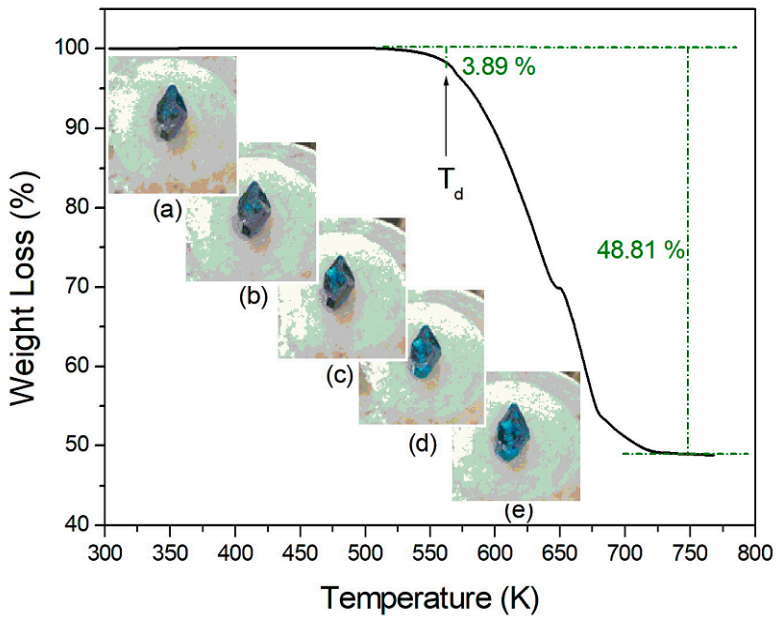

Figure 1. Thermogravimetric analysis (TGA) curve of $(CH_3NH_3)_2CoBr_4$ (inset: states of the crystal at temperatures of (**a**) 300 K, (**b**) 400 K, (**c**) 500 K, (**d**) 550 K, and (**e**) 570 K).

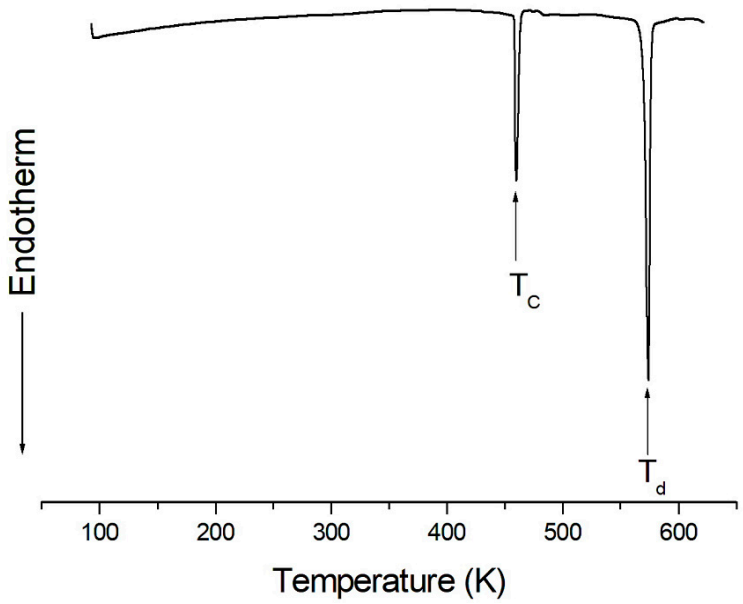

Figure 2. Differential scanning calorimetry (DSC) curve of $(CH_3NH_3)_2CoBr_4$.

The mass loss of 37% near 669 K is likely attributable to the decomposition of the 2HBr moieties. Moreover, the mass loss near 700 K reaches 48.81%. These results are consistent with the TGA results reported by Babu et al. [13]. By the end, only $CoBr_2$ remains. The solid-state decomposition is essentially one of the chemical reactions that occur at the surface. The second stage is associated with the thermal decomposition of $(CH_3NH_3)_2CoBr_4$ to $CoBr_2$. Optical polarizing microscopy showed that the crystals have a seagrass color at room temperature. The color of the crystal does not vary as the temperature increases, and the crystal starts to melt at temperatures above T_d, as indicated at the surface. From the TGA and DSC results, the phase transition temperature is 460 K, and the partial decomposition temperature is at 572 K. The high-temperature phenomenon above T_d is not related to a physical change, such as structural phase transitions, but is instead related to chemical changes, such as thermal decomposition.

The temperature-dependent ^{1}H-NMR spectrum of $(CH_3NH_3)_2CoBr_4$ is obtained to understand and analyze its structure. All recorded spectra contain only one resonance line, and Figure 3 shows the spectrum at 410 K. The spinning sideband for ^{1}H in CH_3 is marked with open circles, and that for ^{1}H in NH_3 is marked with asterisks. The ^{1}H resonance line has an asymmetric shape, and the full-width at half maximum (FWHM) values on the left and right sides are not equal. The asymmetric line shape is attributed to the overlapping lines of the two ^{1}H in the $(CH_3NH_3)^+$ cations. The ^{1}H-NMR chemical shift of $\delta = -0.3$ ppm is due to the CH_3, while the ^{1}H-NMR chemical shift of $\delta = 4.2$ ppm is due to the NH_3. The ^{1}H-NMR chemical shifts for the two ^{1}H in the $(CH_3NH_3)^+$ cations are temperature-independent. They remain quasi-constant with increasing temperature, indicating that the structural environment of ^{1}H in the CH_3 and NH_3 groups does not change.

Figure 4 shows the recovery traces for the ^{1}H resonance lines for delay times that range from 1 μs to 20 ms at 300 K. Herein, the arrows mark the resonance lines at each delay time, while the other resonance lines are the sidebands. The $T_{1\rho}$ values are obtained from the intensities of the magnetization recovery curves with respect to the delay time. The recovery traces are described by a simple mono-exponential function [18–20].

$$P(\tau) = P(0)\exp(-\tau/T_{1\rho}) \quad (3)$$

where $P(\tau)$ is the NMR signal intensity measured after recovery time τ, and $P(0)$ is the total nuclear magnetization of the protons at thermal equilibrium. This analysis method is used to obtain the $T_{1\rho}$ values for the proton in the $(CH_3NH_3)^+$ cations. However, the ^{1}H $T_{1\rho}$ values for CH_3 and NH_3

are indistinguishable owing to the overlapping responses of the two protons. The ^{1}H $T_{1\rho}$ values for $(CH_3NH_3)_2CoBr_4$ obtained herein and the corresponding values for $(CH_3NH_3)_2CdBr_4$ reported previously [17] are shown in Figure 5 as a function of the inverse temperature. In the case of $(CH_3NH_3)_2CoBr_4$, the ^{1}H $T_{1\rho}$ values increased rapidly near 210 K, and those at high temperatures are almost continuous; the $T_{1\rho}$ value at 180 K is 76 μs and that at 300 K is 10 times longer than that at 180 K. The $T_{1\rho}$ value is very short at low temperatures, and thus indicates rapid energy transfer from the nuclear spin system to the surrounding environment. On the other hand, the ^{1}H $T_{1\rho}$ values are obtained for each proton in CH_3 and NH_3 in the case of $(CH_3NH_3)_2CdBr_4$ as a function of reciprocal temperature. Herein, the $T_{1\rho}$ values for the two protons of the $(CH_3NH_3)^+$ cations are nearly the same within experimental error. The $T_{1\rho}$ values of ^{1}H in the CH_3 and NH_3 ions abruptly decrease at approximately 360 K. The ^{1}H $T_{1\rho}$ value of $(CH_3NH_3)_2CoBr_4$ including the paramagnetic ions is very short, whereas that of $(CH_3NH_3)_2CdBr_4$ excluding paramagnetic ions is very long.

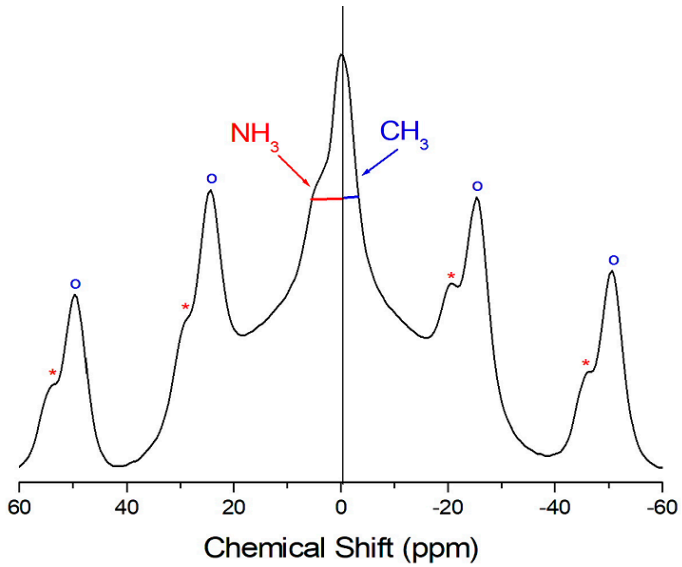

Figure 3. ^{1}H-NMR spectrum for $(CH_3NH_3)_2CoBr_4$ crystal at 410 K. The open circles are the marked sidebands for CH_3 and the asterisks are the marked sidebands for NH_3.

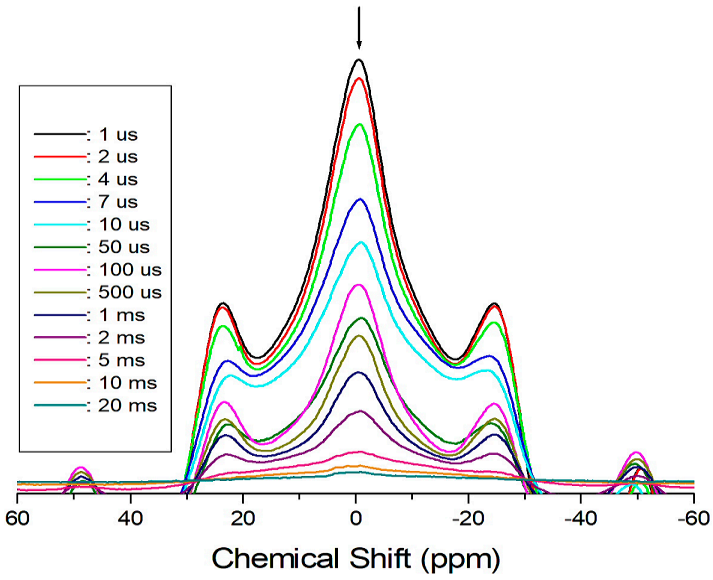

Figure 4. Recovery traces for ^{1}H-NMR spectrum in $(CH_3NH_3)_2CoBr_4$ as a function of delay time from 1 μs to 20 ms.

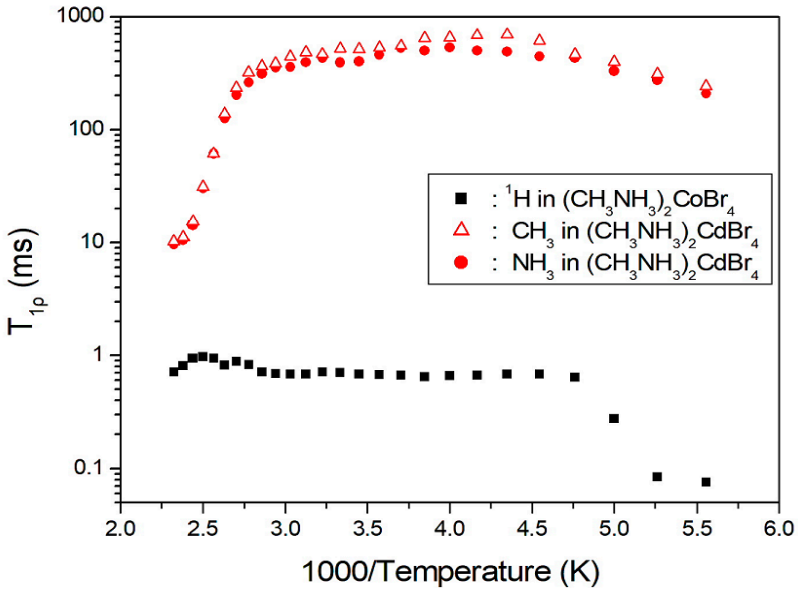

Figure 5. ^{1}H spin–lattice relaxation times in $(CH_3NH_3)_2CoBr_4$ and $(CH_3NH_3)_2CdBr_4$ as a function of inverse temperature.

The local environment of the carbons in $(CH_3NH_3)_2CoBr_4$ was studied by ^{13}C MAS NMR, and the corresponding ^{13}C-NMR chemical shifts are shown in Figure 6. Attention was paid to ^{13}C-NMR, which should be a sensitive probe of the local environment and of the cation dynamics.

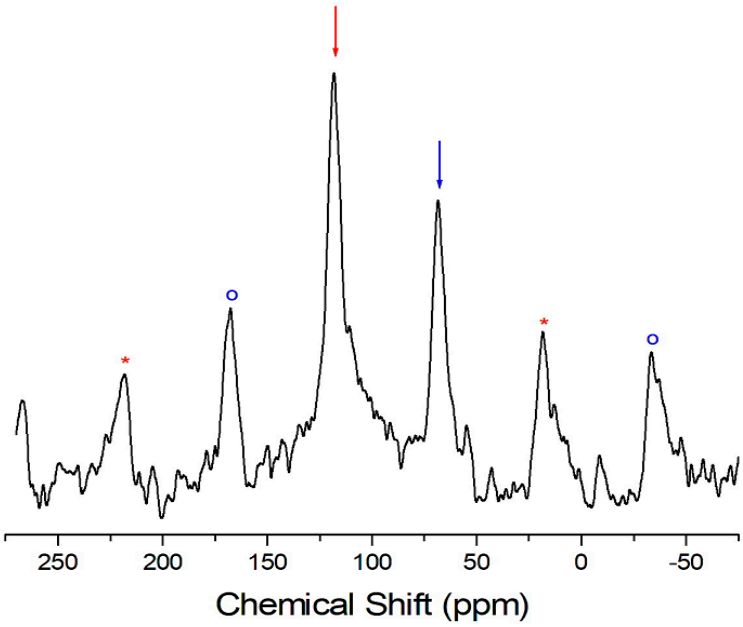

Figure 6. ^{13}C-NMR spectrum in $(CH_3NH_3)_2CoBr_4$ at 300 K. The two arrows denote the signals of the two crystallographically different CH_3 moieties. The spinning sidebands are marked with open circles and asterisks.

The ^{13}C-NMR spectrum at 300 K in $(CH_3NH_3)_2CoBr_4$ shows two signals at the chemical shifts of δ = 68.3 ppm and δ = 117.9 ppm with respect to TMS [21]. The ^{13}C-NMR spectrum consists of two lines that correspond to a-CH_3 and b-CH_3. The signals respectively represent the methyl carbons in the two crystallographically different a-CH_3 and b-CH_3. The ^{13}C-NMR chemical shifts of the two compounds of $(CH_3NH_3)_2CoBr_4$ and $(CH_3NH_3)_2CdBr_4$ are shown in Figure 7 as a function

of temperature. The ^{13}C-NMR chemical shifts vary significantly with temperature. Specifically, the ^{13}C-NMR chemical shifts in the case of $(CH_3NH_3)_2CoBr_4$ decrease slowly and monotonically as a function of temperature. Conversely, the ^{13}C-NMR spectrum at 300 K in $(CH_3NH_3)_2CdBr_4$ shows two signals at chemical shifts of δ = 27.9 ppm and δ = 29.3 ppm. The ^{13}C-NMR chemical shifts of the crystallographically different a-CH_3 and b-CH_3 slowly and monotonously increase as a function of temperature. The ^{13}C chemical shifts of the CH_3 groups differ between the two compounds. Generally, the paramagnetic contribution to the NMR shift is responsible for the NMR spectra. The ^{13}C chemical shift of $(CH_3NH_3)_2CoBr_4$, which contains paramagnetic ions, was significantly different to that of $(CH_3NH_3)_2CdBr_4$, which does not contain paramagnetic ions. The differences in the ^{13}C chemical shifts could potentially be due to differences in the electron structures of the metal ions.

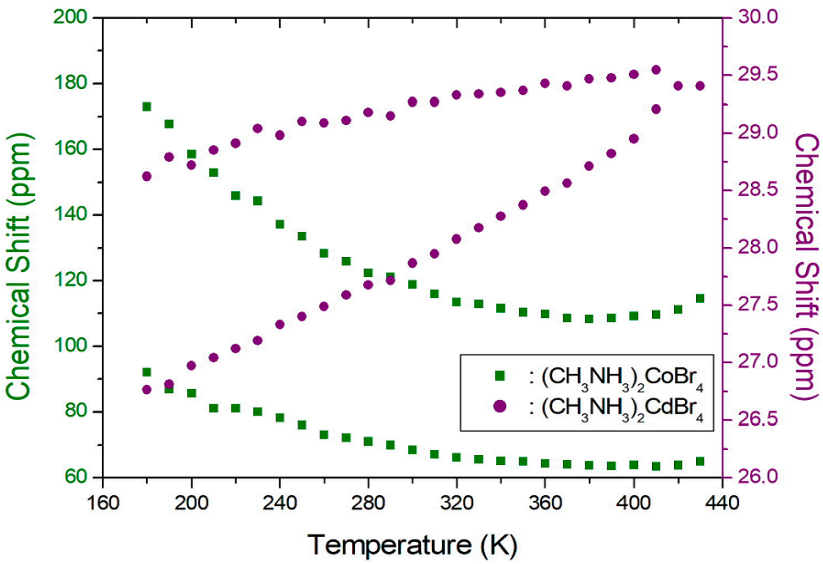

Figure 7. ^{13}C-NMR chemical shifts of $(CH_3NH_3)_2CoBr_4$ and $(CH_3NH_3)_2CdBr_4$ as a function of temperature.

To determine the ^{13}C $T_{1\rho}$, nuclear magnetization was measured as a function of the delay time. The signal intensities of the nuclear magnetization recovery curves are fitted by the mono-exponential function of Equation (3). From these results, $T_{1\rho}$ values were obtained for the carbons in $(CH_3NH_3)_2CoBr_4$ and $(CH_3NH_3)_2CdBr_4$ as a function of the inverse temperature, as shown in Figure 8. In the case of $(CH_3NH_3)_2CoBr_4$, the $T_{1\rho}$ values of ^{13}C show a minimum value near 330 K, while the $T_{1\rho}$ value abruptly decreases above 410 K. The $T_{1\rho}$ values for a-CH_3 and b-CH_3 are also very similar and of the order of 10 ms. Conversely, the variation of $T_{1\rho}$ with temperature in the case of $(CH_3NH_3)_2CdBr_4$ exhibits a minimum near 250 K for a-CH_3 and b-CH_3, respectively, and $T_{1\rho}$ decreases abruptly above 360 K. The presence of these minima are attributed to the effects of the reorientation of $(CH_3NH_3)^+$ cations. From the ^{13}C $T_{1\rho}$ curves, the relaxation processes of $(CH_3NH_3)_2CdBr_4$ are affected by molecular motion described by the Bloembergen–Purcell–Pound (BPP) theory [22]. The experimental values of $T_{1\rho}$ are explained by the correlation time τ_C for molecular motion based on the BPP theory [22,23],

$$(1/T_{1\rho}) = 0.05(\mu_o/4\pi)^2[\gamma_H{}^2\ \gamma_C{}^2\ \hbar^2/r^6][4F_a + F_b + 3F_c + 6F_d + 6F_e] \quad (4)$$

where

$F_a = \tau_C/[1 + \omega_1{}^2\tau_C{}^2]$
$F_b = \tau_C/[1 + (\omega_H - \omega_C)^2\tau_C{}^2]$
$F_c = \tau_C/[1 + \omega_C{}^2\tau_C{}^2]$
$F_d = \tau_C/[1 + (\omega_H + \omega_C)^2\tau_C{}^2]$
$F_e = \tau_C/[1 + \omega_H{}^2\tau_C{}^2]$.

where μ_o is the permeability, γ_H and γ_C are the respective gyromagnetic ratios for the ^1H and ^{13}C nuclei, r is the distance of H–C, $\hbar = h/2\pi$, and ω_H and ω_C are the respective Larmor frequencies of ^1H and ^{13}C.

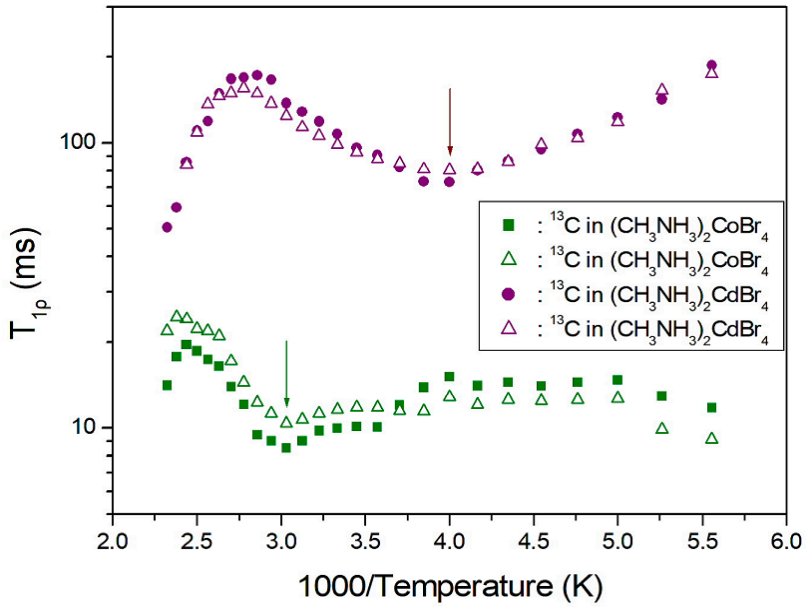

Figure 8. ^{13}C spin–lattice relaxation times of $(CH_3NH_3)_2CoBr_4$ and $(CH_3NH_3)_2CdBr_4$ as a function of inverse temperature.

On the other hand, the relaxation processes of $(CH_3NH_3)_2CoBr_4$ with the paramagnetic Co^{2+} ions are affected by the molecular motion described by the Solomon equation [24]. When paramagnetic ions exist, the $T_{1\rho}$ are represented by τ_C, as presented in [24]

$$(1/T_{1\rho}) = (1/15)(\mu_o/4\pi)^2[\gamma_I^2\gamma_e^2\mu_B^2S(S+1)/r^6][4G_a + G_b + 3G_c + 6G_d + 6G_e] \quad (5)$$

where

$G_a = \tau_C/[1 + \omega_1^2\tau_C^2]$
$G_b = \tau_C/[1 + (\omega_C - \omega_e)^2\tau_C^2]$
$G_c = \tau_C/[1 + \omega_C^2\tau_C^2]$
$G_d = \tau_C/[1 + (\omega_C + \omega_e)^2\tau_C^2]$
$G_e = \tau_C/[1 + \omega_e^2\tau_C^2]$.

Here, γ_e is the gyromagnetic ratio of the electron, S is the total spin quantum number of the paramagnetic ion, and ω_e is the Larmor frequency of the electron. Additionally, ω_1 is the angular frequency at the spin-lock field; 59.52 kHz for $(CH_3NH_3)_2CoBr_4$ and 67.56 kHz for $(CH_3NH_3)_2CdBr_4$. The $T_{1\rho}$ exhibits a minimum when $\omega_1\tau_C = 1$. Based on this condition, the coefficients of Equations (4) and (5) which are dependent on ω_1, ω_H, and ω_C, can be obtained. Furthermore, the value of τ_C can be calculated, and its temperature dependence follows a simple Arrhenius expression [22] according to,

$$\tau_C = \tau_o\exp(-E_a/RT) \quad (6)$$

where τ_o is the preexponential factor, T is the temperature, R is the gas constant, and E_a is the activation energy. The activation energies for the tumbling motion of a-CH_3 and b-CH_3 in the case of $(CH_3NH_3)_2CoBr_4$ are obtained from the log τ_C vs. 1000/T curve, and are respectively equal to 24.51 ± 0.99 kJ/mol and 23.25 ± 1.30 kJ/mol, whereas the corresponding values in the case of $(CH_3NH_3)_2CdBr_4$ are 8.18 ± 0.37 kJ/mol and 7.65 ± 0.21 kJ/mol (see Figure 9). When paramagnetic Co^{2+} ions exist, $1/\tau_C$ =

$1/\tau_r + 1/\tau_M + 1/\tau_e$, where τ_r, τ_M, and τ_e, are the rotational correlation time, exchange correlation time, and electronic relaxation correlation time, respectively. The τ_r can represent molecular motion. For $(CH_3NH_3)_2CdBr_4$, there is no chemical exchange or paramagnetic terms, and so τ_C can directly reflect the molecular motion. In the case of $(CH_3NH_3)_2CoBr_4$, τ_e dominates the total correlation time, and thus, τ_C is not directly related to molecular motion.

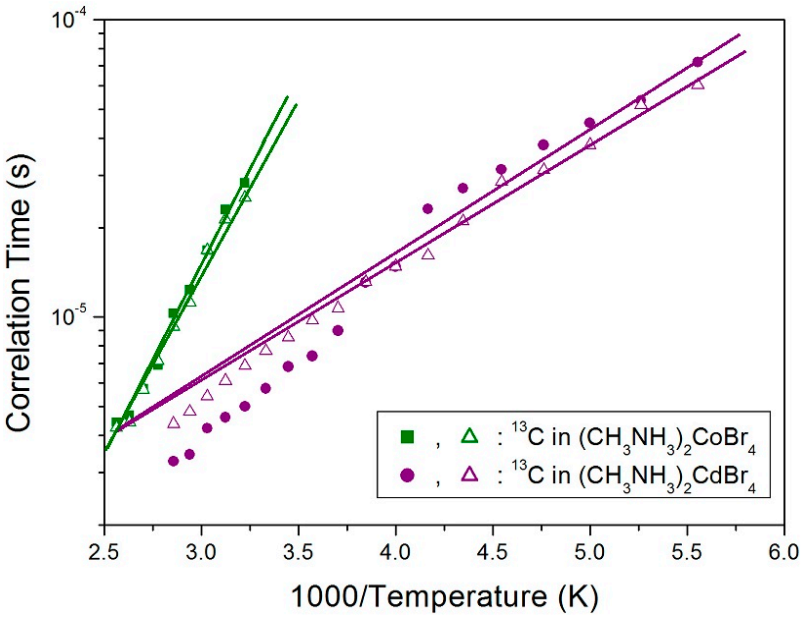

Figure 9. Arrhenius plots of the natural logarithm of the correlation times for each of the carbons of a-CH_3 and b-CH_3 in $(CH_3NH_3)_2CoBr_4$ and $(CH_3NH_3)_2CdBr_4$ as a function of inverse temperature.

3. Materials and Methods

The $(CH_3NH_3)_2CoBr_4$ single crystals were grown based on the slow evaporation of an aqueous solution with a 2:1 ratio of $CH_3NH_2{\cdot}HBr$ and $CoBr_2$ at 300 K. Single crystals have a diamond shape and seagrass color.

The thermal properties and phase transition temperature were measured using a TGA (TA, DSC 25) instrument at a heating rate of 10 °C/min. The TGA and DSC curves were measured in an N_2 atmosphere, and the mass of the powder sample used in the experiment was 9.22 mg.

The solid-state MAS NMR spectra and the spin–lattice relaxation time $T_{1\rho}$ in the rotating frame of $(CH_3NH_3)_2CoBr_4$ crystals were recorded on a Bruker 400 DSX NMR spectrometer (Bruker, Leipzig, Germany) at the Korean Basic Science Institute at the Western Seoul Center. Solid samples were inserted into 4 mm diameter zirconia rotors. The samples were spun at a sufficient speed to avoid spinning sidebands overlapping. The chemical shifts were defined with respect to tetramethylsilane (TMS). The ^1H $T_{1\rho}$ values were measured using a $\pi/2$-τpulse sequence by varying the duration of the spin-locking pulses. The ^{13}C $T_{1\rho}$ values were measured based on the variation of the duration of the ^{13}C spin-locking pulse. The usual experimental approach assumes the use of cross-polarization from protons to enhance the ^{13}C sensitivity. The widths of the $\pi/2$ pulses for ^1H and ^{13}C were 4.1 μs and 4.2 μs, respectively. The $T_{1\rho}$ values were measured in the temperature range of 180–430 K due to limitations of the experimental equipment associated with the measurements of the spectra and $T_{1\rho}$ outside of this range. The sample temperatures were held constant by controlling the helium gas flow and the heater current [25,26].

4. Conclusions

The thermal properties and phase transition temperature of $(CH_3NH_3)_2CoBr_4$ crystals grown based on the slow evaporation method were investigated with TGA, DSC, and optical polarizing microscopy. The phase transition and partial decomposition temperatures were observed at 460 K and

572 K, respectively. The high-temperature phenomenon above 572 K was not related to a physical change like the structural phase transition. Instead, it was related to a chemical change, such as thermal decomposition.

The paramagnetic interactions of $(CH_3NH_3)_2CoBr_4$, associated with the role of the $(CH_3NH_3)^+$ cations were studied by ^{1}H-NMR and ^{13}C-NMR as a function of temperature. The ^{1}H and ^{13}C MAS NMR were used to probe the dynamics of cations in $(CH_3NH_3)_2CoBr_4$ and $(CH_3NH_3)_2CdBr_4$. The chemical shift by the MAS NMR depended on the local field at the site of the resonating nucleus in crystals. The effect of these crystals on the ^{1}H and ^{13}C-NMR chemical shifts was investigated using temperature-dependent NMR experiments. The contributions to the ^{13}C-NMR chemical shifts are correlated with the distribution of spin density in the ligand moiety.

The temperature dependence of the $T_{1\rho}$ values for ^{1}H reflect the modulation of the inter-NH_3 and inter-CH_3 dipolar interactions due to the $(CH_3NH_3)^+$ cations. The variation of $T_{1\rho}$ for ^{13}C yielded a minimum, and it is apparent that the $T_{1\rho}$ values for ^{13}C are governed by tumbling motions. Moreover, the paramagnetic dopant led to the shortening of their $T_{1\rho}$ values. Accordingly, it has been shown that the $T_{1\rho}$ value is inversely proportional to the square of the magnetic moment of the paramagnetic ion [27]. The $T_{1\rho}$ values of ^{1}H and ^{13}C of the $(CH_3NH_3)_2CoBr_4$ crystals, which contain paramagnetic ions, are much shorter than those of the $(CH_3NH_3)_2CdBr_4$ crystals, which do not contain paramagnetic ions.

The $(CH_3NH_3)_2CoBr_4$ and $(CH_3NH_3)_2CdBr_4$ crystals are of the $(CH_3NH_3)_2MX_4$ type, whereas their individual dynamics differ significantly from the dynamic of the cations. The differences between the $T_{1\rho}$ of the $(CH_3NH_3)_2MBr_4$ crystals (M = Co and Cd) are due to the differences between the electron structures of their Co^{2+} and Cd^{2+} ions. These ions screen the nuclear charge from the motion of the outer electrons. The Co^{2+} has unpaired *d* electrons, whereas Cd^{2+} has filled *d* shells. Their NMR properties stem from the differences between the chemical properties of paramagnetic Co^{2+} and non-paramagnetic Cd^{2+} ions. Furthermore, the NMR relaxation of diamagnetic Cd^{2+} ions is most probably driven by dipolar interactions, whereas the relaxation of paramagnetic Co^{2+} ions is mostly driven by interactions with the paramagnetic center.

Author Contributions: A.R.L. interpreted the TGA, DSC, NMR measurements, and designed the research and wrote the manuscript. S.H.K. performed the NMR experiments.

Funding: This research was supported by the Basic Science Research program through the National Research Foundation of Korea (NRF), funded by the Ministry of Education (2018R1D1A1B07041593).

Conflicts of Interest: The authors declare no conflict of interest.

References

1. Chen, Y.; Li, L.; Yerramilli, A.S.; Qu, W.; Song, Y.; Li, N.; Shen, Y.; Alford, T.L. Introduction of nitrogen gas flow and precursor aging process to improve the efficiency of the lead acetate derived $CH_3NH_3PbI_3$ perovskite solar cells. *Sol. Energy Mater. Sol. Cells.* **2019**, *190*, 49–56. [CrossRef]
2. Elseman, A.M.; Shalan, A.E.; Sajid, S.; Rashad, M.M.; Hassan, A.M.; Li, M. Copper-substituted lead perovskite materials constructed with different halides for working $(CH_3NH_3)_2CuX_4$-based perovskite solar cells from experimental and theoretical view. *ACS Appl. Mater. Interfaces.* **2018**, *10*, 11699. [CrossRef] [PubMed]
3. Aramburu, J.A.; Garcia-Fernandez, P.; Mathiesen, N.R.; Garcia-Lastra, J.M.; Moreno, M. Changing the usual interpretation of the structure and ground state of Cu^{2+}-layered perovskites. *J. Phys. Chem. C* **2018**, *122*, 5071–5082. [CrossRef]
4. Ahmad, K.; Ansari, S.N.; Natarajan, K.; Mobin, S.M. Design and synthesis of 1D-polymeric chain based $[(CH_3NH_3)_3Bi_2Cl_9]$n perovskite: A new light absorber material for lead free perovskite solar cells. *Solar Cell* **2018**, *1*, 2405–2409. [CrossRef]
5. Kubicki, D.J.; Prochowicz, D.; Hofstetter, A.; Pechy, P.; Zakeeruddin, S.M.; Gratzel, M.; Emsley, L. Cation dynamics in mixed-cation $(MA)_x(FA)_{1-x}PbI_3$ hybrid perovskites from solid-state NMR. *J. Am. Chem. Soc.* **2017**, *139*, 10055–10061. [CrossRef] [PubMed]
6. Jahandar, M.; Heo, J.H.; Song, C.E.; Kong, K.J.; Shin, W.S.; Lee, J.C.; Im, S.H.; Moon, S.J. Highly efficient metal halide substituted $CH_3NH_3I(PbI_2)_{1-x}(CuBr_2)_x$ planar perovskite solar cells. *Nano Energy* **2016**, *27*, 330–339. [CrossRef]

7. Novotny, J.; Sojka, M.; Komorovsky, S.; Necas, M.; Marek, R. Interpreting the paramagnetiC-NMR spectra of potential Ru(III) metallodrugs: Synergy between experiment and relativistic DFT calculations. *J. Am. Chem. Soc.* **2016**, *138*, 8432–8445. [CrossRef]
8. Cui, X.P.; Jiang, K.J.; Huang, J.H.; Zhang, Q.Q.; Su, M.J.; Yang, L.M.; Song, Y.L.; Zhou, X.Q. Cupric bromide hybrid perovskite heterojunction solar cells. *Synthetic Metals* **2015**, *209*, 247–250. [CrossRef]
9. Chen, Q.; Marco, N.D.; Yang, Y.; Song, T.B.; Chen, C.C.; Zhau, M.; Hong, Z.; Zhou, H.; Yang, Y. Under the spotlight: The organic-inorganic hybrid halide perovskite for optoelectronic applications. *Nano Today* **2015**, *10*, 355–396. [CrossRef]
10. Rao, C.N.R.; Cheetham, A.K.; Thirumurugan, A. Hybrid inorganic-organic materials: A new family in condensed matter physics. *J. Phys. Condens. Matter* **2008**, *20*, 159801.
11. Yadav, R.; Swain, D.; Kundu, P.P.; Nair, H.S.; Narayana, C.; Elizabeth, S. Dielectric and Raman investigations of structural phase transitions in $(C_2H_5NH_3)_2CdCl_4$. *Phys. Chem. Chem. Phys.* **2015**, *17*, 12207–12214. [CrossRef] [PubMed]
12. Pabst, I.; Fuess, H.; Bats, J.W. Structure of monomethylammonium tetrachlorocuprate at 297 and 100 K. *Acta Crystallogr. C* **1987**, *43*, 413–416. [CrossRef]
13. Babu, R.; Vardhaman, A.K.; Dhavale, V.M.; Giribabu, L.; Singh, S.P. MA_2CoBr_4: Lead-free cobalt-based perovskite for electrochemical conversion of water to oxygen. *Chem. Commun.* **2019**, *55*, 6779–6782. [CrossRef] [PubMed]
14. Daub, M.; Stroh, R.; Hillebrecht, H. Synthesis, Crystal structure, and optical properties of $(CH_3NH_3)_2CoX_4$ (X = Cl, Br, I, $Cl_{0.5}Br_{0.5}$, $Cl_{0.5}I_{0.5}$, $Br_{0.5}I_{0.5}$). *Z. Anorg. Allg. Chem.* **2016**, *642*, 268–274. [CrossRef]
15. Roccanova, R.; Ming, W.; Whiteside, V.R.; McGuire, M.A.; Sellers, I.R.; Du, H.H.; Saparov, B. Synthesis, crystal and electronic structures, and optical properties of $(CH_3NH_3)_2CdX_4$ (X = Cl, Br, I). *Inorg. Chem.* **2017**, *56*, 13878–13888. [CrossRef] [PubMed]
16. Altermatt, D.; Arend, H.; Niggli, A.; Petter, W. New tetrahedrally coordinated A_2CdBr_4 compounds (A = Cs, CH_2NH_3). *Mater. Res. Bull.* **1979**, *14*, 1391–1396. [CrossRef]
17. Lim, A.R. Molecular dynamics of cations and anions by ^{1}H MAS NMR, ^{13}C CP/MAS NMR, ^{14}N NMR, and ^{113}Cd NMR in hybrid organic-inorganic $(CH_3NH_3)_2CdBr_4$. *J. Mol. Structure* **2018**, *1167*, 255–260. [CrossRef]
18. Koenig, J.L. *Spectroscopy of Polymers*; Elsevier: New York, NY, USA, 1999.
19. Mcbrierty, V.J.; Packer, K.J. *Nuclear Magnetic Resonance in Solid Polymers*; Cambridge University Press: Cambridge, UK, 1993.
20. Abragam, A. *The Principles of Nuclear Magnetism*; Oxford University Press: Oxford, UK, 1961.
21. Charles, J.P.; Jacqlynn, B. *The Aldrich Library of ^{13}C and ^{1}H FT NMR Spectra*; Aldrich Chemical Company: Saint Louis, MI, USA, 1993.
22. Bloembergen, N.; Purcell, E.M.; Pound, R.V. Relaxation effects in nuclear magnetic resonance absorption. *Phys. Rev.* **1948**, *73*, 679–712. [CrossRef]
23. Lim, A.R. Role of NH_4 ions in successive phase transitions of perovskite type $(NH_4)_2ZnX_4$ (X= Cl, Br) by ^{1}H MAS NMR and ^{14}N NMR. *RSC Advances* **2018**, *8*, 11316–11323. [CrossRef]
24. Solomon, I. Relaxation processes in a system of two spins. *Phys. Rev. B* **1955**, *99*, 559–565. [CrossRef]
25. Aliev, A.E.; Harris, K.D.M. Simple technique for temperature calibration of a MAS probe for solid-state NMR spectroscopy. *Mag. Reson. Chem.* **1994**, *32*, 366–369. [CrossRef]
26. Langer, B.; Schnell, I.; Spiess, H.W.; Gimmer, A.-R. Temperature calibration under ultrafast MAS conditions. *J. Mag. Reson.* **1999**, *138*, 182–186. [CrossRef] [PubMed]
27. Kubicki, D.J.; Prochowicz, D.; Pinon, A.; Stevanato, G.; Hofstetter, A.; Zakeeruddin, S.M.; Gratzel, M.; Emsley, L. Doping and phase segregation in Mn^{2+}- and Co^{2+}- doped lead halide perovskite from ^{133}Cs and ^{1}H-NMR relaxation enhancement. *J. Mater. Chem. A* **2019**, *7*, 2326–2333. [CrossRef]

Sample Availability: Samples of the compounds $(CH_3NH_3)_2CoBr_4$ are available from the authors.